Accurate Analysis of the Mode (de)multiplexer Using Asymmetric Directional Coupler

C. Pan, and B. M. A. Rahman, *Fellow, IEEE*

Abstract—Design optimizations of asymmetric directional couplers for the fundamental quasi-TE (TM) mode with the higher order quasi-TE (TM) modes (de)multiplexer including the H_y^{21} (H_x^{21}), H_y^{31} (H_x^{31}), H_y^{41} (H_x^{41}), and H_y^{51} (H_x^{51}) modes are studied by a full-vectorial H-field finite element method. Phase matching of non-identical nanowires are more critical and accuracy of the numerical method for the design is tested here. The effect of possible fabrication tolerance is also discussed thoroughly. These results show that a narrow separation of 100 nm or similar value should be employed for the quasi-TE mode splitters, but for the quasi-TM modes, a relatively wide separation of ~ 500 nm can be used. The fabrication of the single mode nanowire should be strictly accurate within ± 5 nm of the design values.

Index Terms—Silicon photonics, mode (de)multiplexer, asymmetric directional coupler, finite element analysis.

I. INTRODUCTION

A series of technological breakthroughs such as WDM, advanced coding technique had allowed the capacity per fiber to be increased around ten fold every four years in the past [1]. However, the capacity of the optical communication systems based on these transmission technologies is going to be saturated and will not be able to keep up with the exponential growth of the Internet traffic. It is possible that the bandwidth bottleneck may be effectively alleviated by the mode-division multiplexing (MDM) technique with the introduction of few-mode fibers [2-4]. Early study has shown a transmission capacity of 960 Gb/s per wavelength through three LP modes with a few-mode fiber [4]. Especially, in comparison with WDM system, MDM system is relatively cheap and compatible solution of optical interconnects for parallel chip multiprocessors [5]. One laser diode is needed in MDM system, so it contributes less to the power consumption of electric chips which are power sensitive.

Mode (de)multiplexer is one of the key devices in MDM system. Several types of mode (de)multiplexer with different materials and structures have been proposed [6-18]. Compact mode (de)multiplexer based on Silicon-om-insulator (SOI) is

more attractive and convenient for design, because the conversion between higher order modes and the fundamental mode could be realized through the coupling between close planar guides, and several solutions are proposed to solve the insertion issues between Silicon planar integrated circuit (PIC) and fiber [19-22]. SOI mode (de)multiplexers using asymmetric Y junction or tapered asymmetrical directional couplers (ADCs) based on mode evolution have been demonstrated [12-16]. However, their fabrication is a big problem because a smooth tapered structure is still difficult to achieve precisely now. Alternatively, ADC based mode (de)multiplexer [17-18] can be low-loss, low-crosstalk and high scalability for more mode channels. The channel can be added through direct cascade. Although an 8-channel mode multiplexer based on asymmetric directional coupler has been fabricated and tested experimentally [18], the design optimization of the parameters and performance analysis of fabrication tolerance of the ADC section using more accurate numerical method are still missing.

In this paper, design optimization of the ADC for SOI mode (de)multiplexer is presented by using a full-vectorial **H**-field finite element method (FEM). The width of multi-mode nanowire is optimized following the phase matching condition. As a result, the fundamental mode of access single mode nanowire (SMNW) can be converted to higher order mode and coupled to the multi-mode nanowire (SMNW). Separation between these two nanowires is determined through tolerance analysis which is simulated by the least-squares boundary residual (LSBR) method. The influence of fabrication tolerances is also discussed thoroughly in this paper. The result shows that the narrow separation of 100 nm should be employed and the fabrication of the SMNW should be strictly accurate with the error of less than ± 5 nm as the structure is very sensitive to the change of nanowire (NW) width.

II. THEORY

The number of guided modes and the propagation constants of these modes increase as the width of the SOI NW increases. For symmetric directional coupler, the width of the waveguides are identical, and as a result, power may transfer from one waveguide to the other naturally. It should be noted that for identical coupler, power cannot be exchanged between two different modes. For an ADC, power between the two guides can transfer only when these modes are phase matched and this possible when these guides are of nonidentical widths. Based on this phenomenon, mode (de)multiplexer can be realized by ADC structure. For the mode (de)multiplexer, the fundamental

mode in a SMNW will be converted into the higher order mode and coupled into a SMNW when their propagation constants equal to each other or very close. Therefore, an accurate numerical approach is needed to obtain the precise mode condition of these two NWs for the design. On the other hand, as to all practical optical waveguide with 2D confinement, the eigen modes are classified as quasi-TE and quasi-TM modes, and all the contain six components of the **E** and **H** fields. Thus, a full-vectorial numerical method should be used to find accurate eigen modes in these NWs.

The full-vectorial numerical method used here is an **H**-field based FEM, one of the most accurate and numerically efficient approaches. The formulation is based on the minimization of the full **H**-field energy functional [23],

$$\omega^2 = \frac{\iint [(\nabla \times \boldsymbol{H})^* \cdot \hat{\varepsilon}^{-1} (\nabla \times \boldsymbol{H}) + p (\nabla \cdot \boldsymbol{H})^* (\nabla \cdot \boldsymbol{H})] dxdy}{\iint \boldsymbol{H}^* \cdot \hat{\mu} \boldsymbol{H} dxdy} \quad (1)$$

where **H** is the full-vectorial magnetic field, * denotes a complex conjugate and transpose, ω^2 is the eigenvalue (ω being the angular frequency), p is a weighting factor for penalty term to eliminate spurious modes and $\hat{\varepsilon}$ and $\hat{\mu}$ are permittivity and permeability tensors, respectively. This full-vectorial FEM is also used to determine the coupling length between the fundamental mode and the higher order modes through calculating the propagation constants of the even and odd supermodes.

The beam propagation method (BPM) [24] is a useful approach to study the evolution of optical waves along z-variant optical structures and calculate the power transfer during modal conversion. However, for an ADC, composed of two butt-coupled uniform NWs with only two discrete interfaces, a junction analysis approach would be numerically more suitable. The least-squares boundary residual (LSBR) method is more accurate than the other available techniques for the analysis of power transfer characteristics in practical guided-wave problems [25]. The LSBR method looks for stationary solution to satisfy the continuity conditions of the tangential **E** and **H** fields in a least squares sense over the interface by minimizing the error energy functional, J, as given [26]

$$J = \int \left| E_t^I - E_t^{II} \right|^2 + a \cdot Z_0^2 \left| H_t^I - H_t^{II} \right|^2 d\Omega \quad (2)$$

where Z_0 is the free-space wave impedance and a is the dimensionless weighting factor to balance the electric and magnetic components of the error functional. The integration is carried out at the junction interface, Ω, between the access and asymmetric Silicon NWs. For the structure with one junction, this method would be more efficient and rigorous than that of the BPM.

III. RESULTS AND DISCUSSION

Design accuracy depends on the solution accuracy, and for any numerical method that depends on the numerical parameters used. For the FEM modal solution of SOI nanowire, accuracy depends on the finite number of elements applied for characterization, and this is tested first. The propagation constant $\beta(\omega)$ obtained from the FE modal solution, and the effective index, n_{eff}, of the nanowire can be calculated by $n_{eff} = \lambda \beta(\omega)/2\pi$, where λ is the operating wavelength. Variation of the effective index, n_{eff} of the fundamental

quasi-TE, H_y^{11}, mode with the number of mesh divisions N × N used to represent the half structure is shown in Fig.1 by a solid blue line. The refractive indices of Silicon and Silica are taken as 3.4754752 and 1.4440236 at the operating wavelength of 1550 nm, respectively. The waveguide under consideration has its width and height, W=400 nm, H=220 nm, respectively. It is obvious that n_{eff} increases rapidly at first and then reaches a constant value asymptotically as N increases. The accuracy of n_{eff} rises to 4th decimal place when using a mesh size of 600×600. Aitken's procedure extrapolation [27] has been used to assess the precision of the modal solution for this structure, which extrapolates from three successive values of n_{eff} with a fixed geometric mesh division ratio in both the transverse dimensions of a waveguide:

$$n_{eff}^\infty = n_{eff(i+1)} - \frac{[n_{eff(i+1)} - n_{eff(i)}]^2}{n_{eff(i+1)} - 2n_{eff(i)} + n_{eff(i-1)}} . \quad (3)$$

The extrapolated values of n_{eff}^∞ is also plotted in Fig.1 by a red solid line. For instance, according to Eq. (3), we calculate Aitken's value from three n_{eff} values of 2.10427, 2.10867, 2.10987 for mesh N=250, 500 and 1000, respectively. The extrapolated value is 2.11032 from these there values. The advantage of introducing Aitken's extrapolation is illustrated clearly in Fig.1.
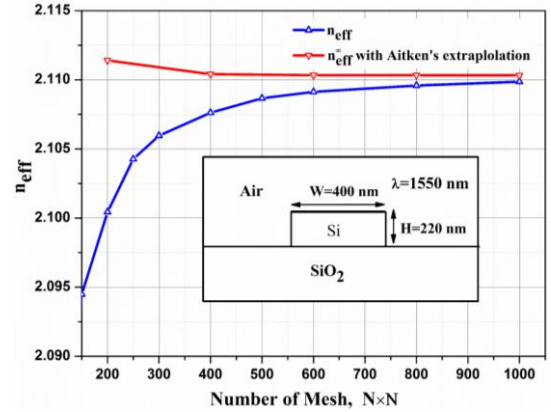

Fig. 1. Variation of n_{eff} of the fundamental quasi-TE H_y^{11} mode with the mesh number (The structure of the SOI NW is shown as an inset).

TABLE I
EFFECTIVE INDICES OF THE H_y^{11} MODE IN SOI NW (W=400 NM) USING VARIOUS NUMERICAL APPROACHES

H-FIELD FEM[23]		COMSOL		Lumerical	
N=500	Aitken's	Coarse	Finer	5	8
2.10867	2.11032	2.10852	2.11069	2.11515	2.11225

We also compared our VFEM results with two commercial software (COMSOL and Lumerical), which are given in Table I. For commercial software often the mesh sizes are classified to different levels. In COMSOL, mesh sizes are classified by coarser, coarse, normal, fine, and finer. In Lumerical, the mesh sizes are divided to Level 1 to Level 8, and the Level 8 is the finest one. With the increase of the mesh size, the effective indices calculated by our method and COMSOL increase to a constant value asymptotically, but the effective index calculated by Lumerical decreases to a constant value. It can be observed from Table I that when using the best mesh size

possible, the effective index values from the VFEM and COMSOL are within 0.02% of each other, but effective index value by Lumerical is about 0.08% higher than that of the two FEM values.

Next, the effect of NW width on the phase matching condition is studied. Variations of the effective indices, n_{eff} of the eigen modes including fundamental quasi-TE H_y^{11} mode, fundamental quasi-TM, H_x^{11}, mode and higher order, H_y^{21}, H_y^{31}, H_x^{21}, H_x^{31}, modes with the width of an isolated SOI NW with height of 220 nm are shown in Fig.2. It can be observed that the effective indices of the all the quasi-TE and quasi-TM modes increase rapidly at first and then asymptotically reach their stable values when the nanowire width increases. The effective index of the quasi-TE mode is bigger than that of the quasi-TM mode of the same order when the width of the nanowire is bigger than its height. The effective indices of any quasi-TE or quasi-TM modes of one guide may be made equal to another
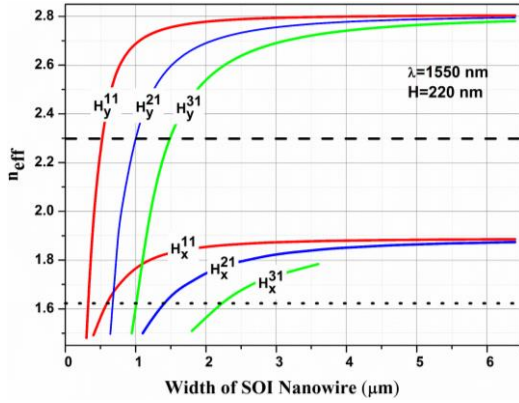

Fig. 2. Variations of the effective indices of eigen modes with the SOI NW width.
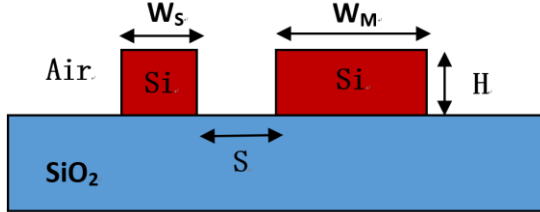

Fig. 3. Diagram of an ADC for mode (de)multiplexer.

mode of a second guide when the value of the effective index value is low, as shown by a black dotted line. However when the value of the effective index is larger enough, for example, bigger than 2.0, *only* quasi-TE modes of SOI nanowire with different specific widths may have the same effective index, indicated by a black dashed line. The second order quasi-TE, H_y^{21} mode approaches its cutoff when the width is lower than 600 nm for H=220 nm. Based on above result, the schematic cross section of ADC for mode (de)multiplexer is shown in Fig.3, consisting of two Silicon nanowire with unequal widths but of equal height, H. All the parameters can be easily controlled by mask design, so it will be easy for fabrication. The width of the SMNW which is used for access is identified by W_S, while the width of the MMNW is identified by W_M. The separation between two waveguides is taken as S.

Accuracy of a design critically depends on the solution accuracy. As we have identified n_{eff} depends on the mesh

used, next accuracy of phase matching is also studied. We calculated the effect of mesh size on defining the width of the MMNW for phase matching with a access SMNW. Variation of the width of MMNW when its H_y^{21} mode is phase matched with the H_y^{11} mode of the SMNW with the width of 400 nm, along the mesh size used and improvement by Aitken's extrapolation are shown in Fig.4, as an example. For mesh size of 200×200, the propagation constant of the SMNW is 8.51799 μm^{-1}, shown by green horizontal line and it suggests W_M should be 827 nm, shown by green slanted line. On the other hand, as the mesh size increased to 400×400, the propagation constant of the SMNW incerases to 8.54453 μm^{-1}, and new phase matching condition sugget that that W_M should be equal to 815 nm, a shift of 12 nm from the former one, shown by a blue slanted line. When the mesh size is increased further to 800×800, the red solid line in Fig.4 shows that the propagation constant of the SMNW is 8.55181 μm^{-1}, the required phase matching width of the MMNW is now 811 nm, with a further shift of 4 nm. We calculated Aitken's value of the propagation constant from three values above as their mesh division ratios are identical, plotted by black slanted line. The propagation constant of SMNW is 8.55456 μm^{-1}, and the phase matching WMNW width needs to be 810 nm, reduced further but by only 1 nm. It can be seen that the phase-matching width decreases as the mesh size increases and the difference between the value of FEM approach with low mesh size of 200×200 and that of more accurate Aitken's extrapolation is about 17 nm. It is clear from this that the accurary of the numerical approach used is very important. As the performance of any ADC critically depends on the accuracy of the phase matching, later on, it will be shown the effect of the solution or fabrication accuracy on the performance. Design by a less accurate methord or less accurate mesh may not be able to achieve expected performance, and a viable design.
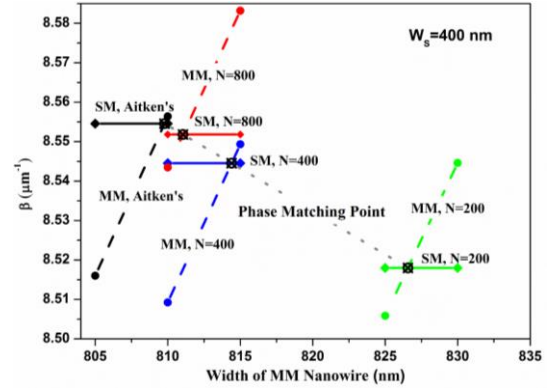
Fig. 4. Variation of the phase-matching point between the H_y^{21} and H_y^{11} modes with the mesh number.

The phase-matching widths for the H_y^{31}, H_y^{41}, and H_y^{51} modes with the H_y^{11} mode, and H_x^{21}, H_x^{31}, H_x^{41} and H_x^{51} modes with the H_x^{11} mode are also calculated by using the Aitken's extrapolation and shown in Tables II and III. The phase matching width of H_y^{31} mode MMNW is 1238 nm when the width of the SMNW is taken as 406 nm. For the SMNW with the width of 379 nm, the necessary phase matching width of the H_y^{41} mode MMNW is 1551 nm. The result discussed above shows phase matching for isolated guide. When two identical

guides are coupled, they always remain phase matched. However, for two nonidentical but phase matched guides, their phase matching condition changes with their separation due to unequal loading.

An ADC as shown in Fig.3 is considered to achieve phase matching between higher order quasi-TE or quasi-TM modes and the fundamental quasi-TE or quasi-TM mode. First, We consider phase matching between H_y^{21} mode in MMNW and H_y^{11} mode in SMNW as an example. Variations of the effective indices of the even and odd supermodes with the width of MM

TABLE II
PHASE MATCHING WIDTHS AND COUPLING LENGTHS FOR DIFFERENT HIGHER ORDER H_y MODES AND SEPARATIONS

Separation	MODE	H_y^{21}	H_y^{31}	H_y^{41}	H_y^{51}
	W_S (nm)	400	406	379	
100 nm	W_M (nm)	818	1250	1572	2058
	L_C (μm)	13.773	18.044	14.553	20.187
200 nm	W_M (nm)	811	1240	1554	
	L_C (μm)	31.732	41.702	31.853	
∞	W_M (nm)	810	1238	1551	2043
	L_C (μm)	-	-	-	-

TABLE III
PHASE MATCHING WIDTHS AND COUPLING LENGTHS FOR DIFFERENT HIGHER ORDER H_x MODES AND SEPARATIONS

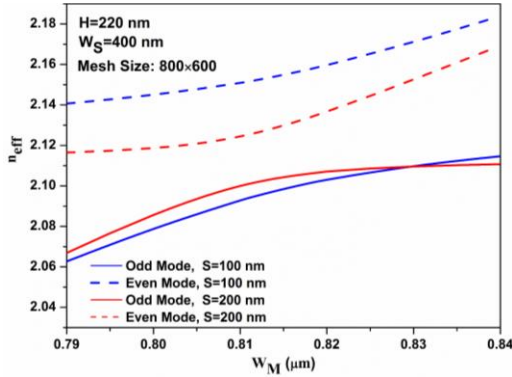| Separation	MODE	H_x^{21}	H_x^{31}	H_x^{41}	H_x^{51}
	W_S (nm)	400	400	400	400
500 nm	W_M (nm)	1100	1754	2442	3088
	L_C (μm)	18.622	22.215	24.772	27.370
700 nm	W_M (nm)	1094	1746	2433	3077
	L_C (μm)	37.585	43.843	47.655	51.497
∞	W_M (nm)	1089	1739	2424	3073
	L_C (μm)	-	-	-	-

Fig. 5. Variations of the effective indices of two supermodes (a) with the width of MMNW, W_M for two different separations, S.

waveguide are plotted in Fig.5 for two different separations. The width of the SMNW is fixed at 400 nm. It is shown that the effective indices of all the modes are increasing with the increase of the MMNW width. Although the effective index curves of even and odd supermodes do not cross each other, transformation from H_y^{11} mode to H_y^{21} mode can take place near the interaction region, where two supermodes show the mixture of H_y^{11} mode and H_y^{21} mode, as shown in Fig.6. For S=200 nm, the H_y^{21} mode of this guide is phase matched with the H_y^{11} mode of the SM nanowire when W_M=811 nm as shown by red lines. However, when the separation is reduced to 100 nm as shown by blue lines, the interactions between the H_y^{11} mode and the H_y^{21} mode are more intense, and as a result, the

gap between these two effective indices near the phase matching is larger and the phase matching width shifts to W_M=818 nm. It is known that for identical coupled guides, the phase matching width remains constant when the separation is changed. However, for nonidentical coupled guides, the phase matching width varies as the mutual loadings of the two guides are different for different separations. The phase matching widths for the H_y^{31}, H_y^{41}, H_y^{51}, with the Hy11 mode and H_x^{21}, H_x^{31}, H_x^{41}, H_x^{51} modes with the H_x^{11} mode are shown in Tables II and III. We can also observe from Table II and III that the width of phase-matching MM nanowire will increase with the reduction of the separation for both polarization modes. In comparasion with the similar work of another group[17][18], their designs show the phase matching MMNW widths for the H_y^{21} mode, the H_y^{31} mode, and the H_y^{41} mode cases are 835 nm, 1238 nm, 1631 nm, respectively, and the width of SMNW for each case is the same as ours. It can be observed that the phase matching MMNW width used in their designs is significantly larger than ours, particularly for the H_y^{41} mode case. According to our study shown above, low separation and low mesh size for the FEM may cause the increase of the phase matching MMNW width. Although the waveguide seperations in their designs are not given, but it is most likely that a low mesh refinement may have been used which can explain the reason for their required phase martching width being wider than ours. On the other hand, as to the fundamental quasi-TM mode and the higher order quasi-TM mode (de)multiplexer, their designs show the phase matching MMNW widths for the H_x^{21} mode, the H_x^{31} mode, and the H_x^{41} mode cases are 1035 nm, 1695 nm, 2363 nm, respectively which are much narrower than our result, and the width of SMNW in each case is also the same as ours. It was observed that the phase matching widths for isolated quaisi-TM modes increases as the finer mesh is used.

The 2-D H_y field contours of the two supermodes in the ADC are given as insets in Fig.6, when the H_y^{21} mode in the MMNW is phase matching to the H_y^{11} mode in the SMNW. In this case the width of SMNW is 400 nm and for separation of 100 nm the phase matching width of the MMNW is 818 nm. The left and right guides in both the insets are SM and MM
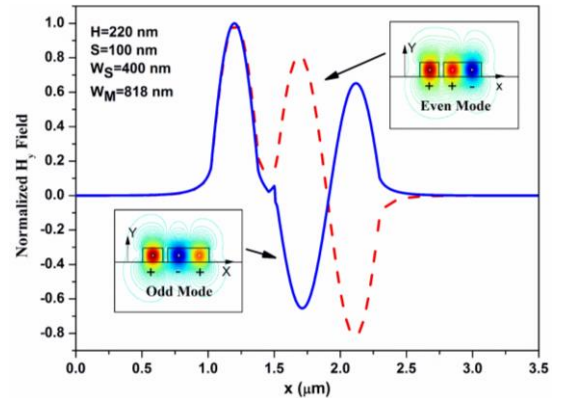

Fig. 6. Normalized H_y field of even and odd supermodes in the ADC for H_y^{21} mode and H_y^{11} mode (de)multiplexer.

guides, respectively. The inset in the lower left shows the odd supermode field profile, where sign of field is inverted at the interface when the H_y^{11} and the H_y^{21} modes merge. The even

supermode field profile is shown in the upper right inset, and the sign of the field remains the same at the interface. In order to show the magnitude of the field clearly, field profile of the even and odd supermodes in the center of the guides along the X-direction (Width-direction) are shown by a blue solid line and a red dashed line, respectively. For phase matching condition, the power in each guide must be very similar. As the width of MMNW is bigger than that of SMNW, it can be
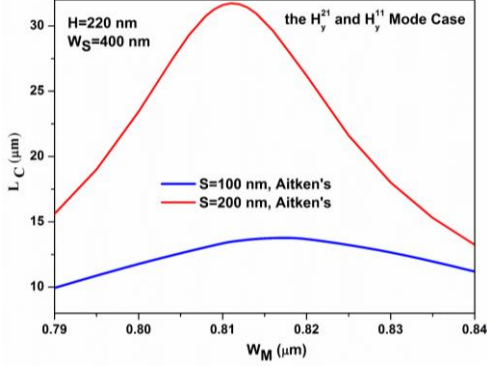

Fig. 7. Variations of the coupling length, L_C with the width of MMNW, W_M for two different separations, S, in the H_y^{21} mode and H_y^{11} mode (de)multiplexing case.

observed that the peak of the H_y^{21} part of the field of the two supermodes is smaller than that of the H_y^{11} peak in the left guide.

The coupling lengths from the propagation constants of the two supermodes are also calculated. Variations of the coupling length, L_C with the width of the H_y^{21} mode guide for S=200 nm and S=100 nm are shown in Fig.7. It can be observed that the coupling length reaches its peak at the phase matching width because the difference between the effective indices of the two supermodes are minimum there. The coupling length is longer and its variation with the width of the MMNW, W_M becomes sharper when the separation is increased. Therefore, for narrower separation, not only the coupling length is shorter, but it would be also less sensitive to the changes in the MMNW width. We also calculated the variations of the coupling length,

L_C with the width of the H_x^{21} mode guide for different separations, which is not shown here. For the H_x mode case, a wider separation of 500 nm can be adopted. Table sII and III list the coupling lengths for different higher order modes and separations when satisfying the phase matching condition.

After calculating the widths of MM guides necessary for phase matching, together with the coupling length for the ADCs, the LSBR method is applied to calculate the power transmission of the structure and to evaluate the effect of possible fabrication tolerances. This approach yields the transmitted modal coefficient of the even supermode, C_e, and the odd supermode, C_o, excited in the SMNW and ADC interface to satisfy the continuity of the tangential Electric and Magnetic fields. The ADC section of H_y^{11} mode and H_y^{21} mode (de)multiplexer is considered next, as example. Variation of these two supermodes' coefficients with the SMNW width for different separations S_1=100 nm, S_2=200 nm are shown in Fig.8 (a). The phase matching widths of the MMNW for each separation are used in these cases. It can be observed that the coefficient of the even mode increases, and the coefficient of the odd mode decreases, when the SMNW widens. For S_2=200 nm, the values of C_e, C_o are 0.69927 and 0.70730, respectively, at phase matching and are very close to $1/\sqrt{2}$ when both the supermodes carry half power, ideal values for weak coupling. In this case, 99.5% power can be transferred from NW to the ADC. For S_1=100 nm, the values of C_e, C_o are decreased a little to 0.69616 and 0.68406, respectively, at phase matching, and 99% power can be transferred from NW to the ADC. It can be observed that, for larger separation, more power will be transferred. However, it is clear that for smaller separation, C_e, C_o is less sensitive to the change of the SMNW width. Both of these two aspects should be considered for a practical design.

Fig. 9. Variations of the crosstalk, CT and the power of the H_y^{21} mode in the MMNW, P_{tM} with the MMNW width change, $\triangle W_M$ for the fixed and unfixed W_S cases.

W_S (μm)

Fig. 8. Variations of the transimitted modal coefficients C_e, C_o (a) and variations of the normalized output power in the MMNW, P_{tm}, and crosstalk, CT (b) with the width of SMNW, W_S for two different separations, S_1, S_2.

Setting the coupling length, L_C, as the length of the ADC section, Z, two excited supermodes would be out of phase at this distance. As a result, the H_y^{11} mode field in the SMNW will disappear, and instead, the phase-matching higher order mode field in the MMNW will be added up, as a result of vector addition of these two supermodes. The power in each NW can be calculated from the modal coefficients, phase difference and their full vectorial mode profiles. Variations of the power of the H_y^{11} mode in the SMNW and that of the H_y^{21} mode in the MMNW with the change of the SMNW width for different separation S_1, and S_2, are shown in Fig.8 (b). The device length and the MM waveguide width here are kept fixed to the idealized design for each separation. It is shown that the maximum normalized power of the H_y^{21} mode, P_{tM}, in MMNW which indicates the normalized mode conversion power, drawn by red solid and dashed lines are about 0.990 and 0.995 for S_1=100 nm, and S_2=200 nm, respectively. It means more than 99% power of the input H_y^{11} mode wave in SMNW is converted to the H_y^{21} mode wave in MMNW successfully. The minimum amount of the normalized unconverted H_y^{11} mode power in the SMNW which would be defined as crosstalk, CT, plotted by blue solid and dashed lines, and these are about -20.01 dB and -23.52 dB for S_1=100 nm, and S_2=200 nm, respectively. It can also be observed that the variation of the SMNW width away from the ideal phasing matching width will cause a significant deterioration of the performance, especially for a wide separation. For $\pm$10 nm fabrication error, P_{tM} will reduce to 0.611 and 0.009 for S_1=100 nm, and S_2=200 nm, respectively. Therefore, the structure with the narrow separation should be chosen for design, as its performance is less sensitive than that of the one with a wider separation. It is clear that when the fabrication error of the SM guide is less than $\pm$5 nm, the P_{tM} value is reduced by only ~ 10%, while CT increases to -9.7dB. Here, it should be noted the importance of the design accuracy. If the numerical method suggest a design which is inaccurate by 10 nm, even when fabrication was perfect, the performance will be deteriorated as illustrated here.
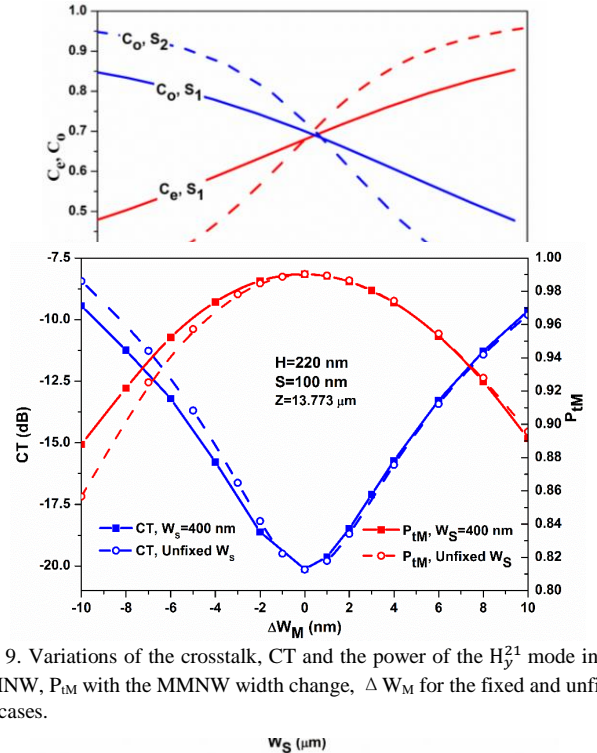
Variations of the crosstalk, CT and the power of the H_y^{21} mode in the MMNW, P_{tM} with the MMNW width change, Δ WM for the fixed and unfixed W_S cases. Here, the separation is taken as 100 nm for the two cases. The length of the ADC section is fixed at the coupling length of phase matching condition, Z=13.773 μm. It can be observed that the decrease of P_{tM} is less than 12%, while CT rises to about -9.4 dB when the width is changed by 10 nm for the fixed W_S case. For the unfixed case, with the 10 nm width variation of SMNW and MMNW, P_{tM} decreases to 0.86, and CT increases to -8.4 dB. It can be also observed that the value of P_{tM} and CT for the two cases are almost the same when the width of MMNW are larger than the optimal value. However, as to the negative change, the deterioration are more terrible for the unfixed W_S case, and the difference of the P_{tM} and CT for the two cases enlarges when the absolute value of the width error increases. Compared with the performance deterioration caused by the width variation of SMNW shown in Fig.8, it is less terrible when SMNW and MMNW have the same width change.

Next, in order to evaluate the influence of random NW width change, Two 2-D contours, Fig.10 (a) and (b) are used to show
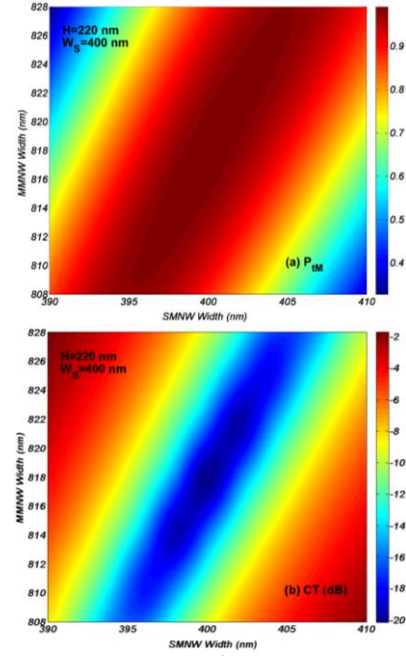

Fig. 10. Variations of the power of H_y^{21} mode in the MM waveguide, P_{tM} (a) and the crosstalk, CT (b) with the width of SMNW and MMNW.
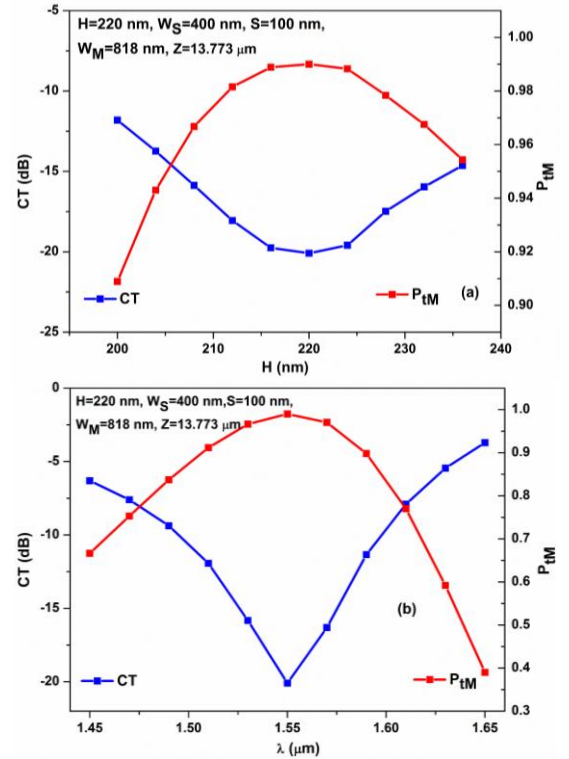

Fig. 11. Variations of the crosstalk, CT and the power of H_y^{21} mode in the MM waveguide, P_{tM} with the height of the waveguides, H (a) and the operating wavelength (b).

the variations of the power of the H_y^{21} mode in the MMNW, P_{tM} and the crosstalk, CT of the ADC with the width change of SMNW and MMNW within $\pm$ 10nm, respectively, which give the result for all possible combination of SMNW and MMNW width changes. It can be observed that with the increase of MMNW width, the SMNW width at which P_{tM} reaches its

maximum value and CT reaches its minimum value also increases, but with smaller width value. Here, the variation range of NW width within which the P_{tM} is bigger than ~ 0.9 and the CT is less than ~ -10 dB is defined as the efficient variation range. It is shown that for any MMNW width in Fig. 10 (a) and (b), the efficient variation range of SMNW width is nearly 10 nm, but with the increase of SMNW width, the efficient variation range of MMNW increases at first, and then decreases after reaching its peak value (~ 20 nm) at the optimal value (W_S=400 nm). It can be also observed that the contours in both the figures are oval which also indicates that the structure is more sensitive to the change of SMNW width.

The deterioration caused by fabrication error of the separation is also analyzed, but not shown here. The value of P_{tM} decreases by only 3%, and CT is better than -14 dB for $\pm$10 nm fabrication error. Regarding the change in the separation, the performance of the structure is stable and insensitive to the mild variation of this parameter.

After evaluting the performance with the changes of widths, the fabrication tolerance of the ADC section height is also studied. Variations of the power of crosstalk, CT, and the power of the H_y^{21} mode, P_{tM}, in the MM waveguide with the change of the height are shown is Fig.11 (a). It is shown that for the fixed length case, Z=13.773 μm, the P_{tM} and CT deteriorates by less than 5% and 5 dB, for $\pm$10 nm fabrication error, respectively.

The effect of operating wavelength variations on the performance of the ADC section is also studied and shown in
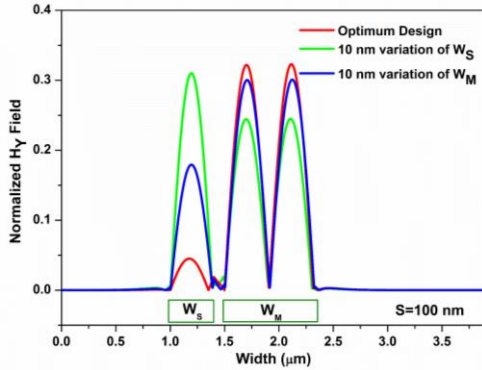

Fig. 12. Normalized H_y field shape along the width axis on the input and output sides of the ADC section with the most idealized and the worst parameters.

Fig. 13. Variations of the crosstalk, CT and the power of the H_y^{31} mode in the MMNW, P_{tM} with the MMNW width, W_M.

Fig.11 (b). It is shown that the crosstalk, CT, is better than -10

dB in a ~ 50 nm wavelength bandwidth.

In order to show the effect of fabrication error more clearly, we plotted the shape of the $|H_y|$ field at the output sides of the ADC section with the optimal and the worst parameters in Fig.12. It is clear that most of the power of the input H_y^{11} mode in the SMNW is converted to the H_y^{21} mode in the MMNW efficiently for the optimum design, as shown by a red line. A small residual field in the SMNW is also visible. However, for a possible change in W_M by 10 nm, which could be due to fabrication error, the converted mode profile is shown by a blue line. After that, the converted mode profile is also shown by a green line when W_S is changed by 10 nm. It can be observed directly that the performance slightly deteriorates to the change of the MM guide width, but suffers larger deterioration to the variation of the SM guide width.

We also evaluated the performance deterioration due to fabrication tolerances of the ADC section for the H_y^{11} mode and H_y^{31} mode (de)multiplexer. Variations of the power of the H_y^{11} mode in the SM waveguide and that of the H_y^{31} mode in the MM waveguide with the change of the MM waveguide width are shown in Fig.13, as an example. In this case, the width of the SMNW and separation are taken as 406 nm and 100 nm, respectively. It is shown that the decrease of the P_{tM} is about 15%, and CT deteriorates to about -8.40 dB when the width is changed by 10 nm.

IV. CONCLUSION

The asymmetric directional coupler for SOI mode (de)multiplexer presented here only contains two simple straight Silicon nanowires, so it will be easy to be fabricated. Multiple channel modes (de)multiplexer can be realized through cascade of a series of asymmetric directional couplers [18].

A detailed design optimization of asymmetric directional sections for the fundamental quasi-TE (TM) mode and the higher order quasi-TE (TM) mode (de)multiplexer including the H_y^{21} (H_x^{21}), H_y^{31} (H_x^{31}), H_y^{41} (H_x^{41}), and H_y^{51} (H_x^{51}) modes is reported. The accurate width of the MMNW is found by FE M approach. The performance deterioration due to fabrication errors is discussed in depth by varying key NW parameters, including the widths, separation, and height. For quasi-TE mode, a narrow separation of 100 nm should be employed for robust design, which will be less sensitive to the slight fluctuation of the separation, the width of the MMNW, and its height, which may satisfy fabrication tolerance condition of $\pm$10nm. On the other hand, for quasi-TM mode, a relatively wider separation of 500 nm can be adopted. It should be noted that the structure is significant sensitive to the change of the SM nanowire width, as the crosstalk CT increases to -4 dB for fabrication error of $\pm$10 nm. The fabrication of SM guide is required to be strictly accurate, which should be less than $\pm$5nm. It is also shown that operating bandwidth of the structure is wide enough and suitable for WDM applications. It is also shown here, accuracy of the design must be tested rigorously and if not careful the design may not be viable.
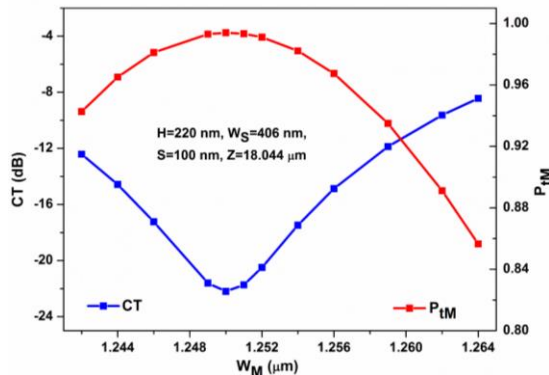
REFERENCES

[1] D. J. Richardson, J. M. Fini and L. E. Nelson, "Space-division multiplexing in optical fibres," Nature Photon., vol. 7, no. 5, pp. 354–362, Apr. 2013.

[2] S. Randel, R. Ryf, A. Sierra, P. J. Winzer, A. H. Gnauck, C. A. Bolle, R.-J. Essiambre, D. W. Peckham, A. McCurdy, and R. Lingle, "6× 56-Gb/s mode-division multiplexed transmission over 33-km few-mode fiber enabled by 6× 6 MIMO equalization," Opt. Express, vol. 19, no. 17, pp. 16697–16707, 2011.

[3] R. Ryf, S. Randel, A. H. Gnauck, C. Bolle, A. Sierra, S. Mumtaz, M. Esmaeelpour, E. C. Burrows, R.-J. Essi-ambre, P. J. Winzer, D. W. Peckham, A. H. McCurdy, and R. Lingle, "Mode-division multiplexing over 96 km of few-mode fiber using coherent 6 × 6 MIMO processing," J. Lightwave Technol., vol. 30, no. 4, pp. 521–531, Feb. 2012.

[4] V. A. J. M. Sleiffer, P. Leoni, Y. Jung, J. Surof, M. Kuschnerov, V. Veljanovski, S. U. Alam, D. J. Richardson, L. Grüner-Nielsen, Y. Sun, B. Corbett, R. Winfield, S. Calabrò, and H. de Waardt, "20 × 960-Gb/s Space-division-multiplexed 32QAM transmission over 60 km few-mode fiber," Opt. Express, vol. 22, no. 1, pp. 749–755, 2014.

[5] A. Shacham, K. Bergman, and L. P. Carloni, "Photonic networks-on-chip for future generations of chip multiprocessors," IEEE Trans. Comput., vol. 57, no. 9, pp. 1246–1260, Sept. 2008.

[6] N. Riesen and J. D. Love, "Weakly-guiding mode-selective fiber couplers," IEEE J. Quantum Electron., vol. 48, no. 7, pp. 941–945, July. 2012.

[7] J. D. Love and N. Riesen, "Mode-selective couplers for few-mode optical fiber networks," Opt. Lett., vol. 37, pp. 3990–3992, 2012.

[8] M.-Y. Chen and J. Zhou, "Design of add-drop multiplexer based on multi-core optical fibers for mode-division multiplexing," Opt. Express, vol. 22, no. 2, pp. 1440–1451, 2014 .

[9] N. Hanzawa, K. Saitoh, T. Sakamoto, T. Matsui, K. Tsujikawa, M. Koshiba, and F. Yamamoto, "Two-mode PLC-based mode multi/demultiplexer for mode and wavelength division multiplexed transmission," Opt. Express, vol. 21, no. 22, pp. 25752–25760, 2013.

[10] N. Hanzawa, K. Saitoh, T. Sakamoto, T. Matsui, K. Tsujikawa, M. Koshiba, and F. Yamamoto, "Mode multi/demultiplexing with parallel waveguide for mode division multiplexed transmission," Opt. Express, vol. 22, no. 24, pp. 29321–29330, 2014.

[11] N. Riesen and J. D. Love, "Tapered velocity mode-selective couplers," J. Lightw. Tech., vol. 31, no. 13, pp. 2163–2169, 2013.

[12] Y. Ding, J. Xu, F. Da Ros, B. Huang, H. Ou, and C. Peucheret, "On-chip two-mode division multiplexing using tapered directional coupler-based mode multiplexer and demultiplexer," Opt. Express, vol. 21, no. 8, pp. 10376–10382, 2013.

[13] M. W. Pruessner, J. B. Khurgin, T. H. Stievater, W. S. Rabinovich, R. Bass, J. B. Boos, and V. J. Urick, "Demonstration of a mode-conversion cavity add-drop filter," Opt. Lett., vol. 36, no.12 , pp. 2230–2232, 2011.

[14] J. B. Driscoll, R. R. Grote, B. Souhan, J. I. Dadap, M. Lu, and R. M. Osgood., "Asymmetric Y junctions in silicon waveguides for on-chip mode-division multiplexing," Opt. Lett., vol. 38, no.11, pp. 1854–1856, 2013.

[15] S. Martínez-Garaot, S.-Y. Tseng, and J. G. Muga, "Compact and high conversion efficiency mode-sorting asymmetric Y junction using shortcuts to adiabaticity," Opt. Lett., vol. 39, no. 8, pp. 2306–2309, 2014.

[16] B. A. Dorin and W. N. Ye, "Two-mode division multiplexing in a silicon-on-insulator ring resonator," Opt. Express, vol. 22, no. 4, pp. 4547–4558, 2014.

[17] D. Dai, J. Wang, Y. Shi, "Silicon mode (de)multiplexer enabling high capacity photonic networks-on-chip with a single-wavelength-carrier light," Opt. Lett., vol. 38, no. 9, pp. 1422–1424, 2013.

[18] J. Wang, P. Chen, S. Chen, Y. Shi, and D. Dai, "Improved 8-channel silicon mode demultiplexer with grating polarizers," Opt. Express, vol. 22, no. 11, pp. 12799–12807, 2014.

[19] B. M. A. Rahman, W. Boonthittanont, S. S. A. Obayya, T. Wongcharoen, E. O. Ladele, and K. T. V. Grattan, "Rigorous Beam Propagation Analysis of Tapered Spot-Size Converters in Deep-Etched Semiconductor Waveguides," J. Lightwave Technol., vol. 21, no. 12, pp. 3392–3398, 2003.

[20] S. Haxha, E. O. Ladely, M. Mjeku, F. AbdelMalek, and B. M. A. Rahman, "Optimization of compact lateral, vertical, and combined tapered spot-size converters by use of the beam-propagation method," Appl. Opt., vol. 45, no. 2, pp. 288-296, 2006.

[21] Y. Fu, T. Ye, W. Tang, and T. Chu, "Efficient adiabatic silicon-on-insulator waveguide taper," Photon. Res., vol. 2, no. 3, pp. A41–A44, 2014.

[22] H. Chen, T. Koonen, B. Snyder, X. Chen, and G. T. Reed. Packaged Mode Multiplexer based on Silicon Photonics. Presented at Asia Communications and Photonics Conference. [Online]. Available: https://www.osapublishing.org/abstract.cfm?URI=ACPC-2012-ATh2B.4

[23] B. M. A. Rahman and J. B. Davies, "Finite element solution of integrated optical waveguides," J. Lightwave Technol., vol. 2, no. 5, pp. 682–688, Oct. 1984.

[24] S. S. A. Obayya, B. M. A. Rahman, and H. A. El-Mikati, "New Full-Vectorial Numerically Efficient Propagation Algorithm Based on the Finite Element Method," J. Lightwave Technol., vol. 18, no. 3, pp. 409–415, 2000.

[25] M. Rajarajan, B. M. A. Rahman, T. Wongcharoen, C. Themistos, N. Somasiria, S. Haxha, and K. T. V. Grattan, "Review of finite-element characterization of photonic devices," J. MOD. OPTIC., vol. 50, no. 12, pp. 1835-1848, 2002.

[26] B. M. A. Rahman and J. B. Davies, "Analyses of optical waveguide discontinuities," J. Lightwave Technol., vol. LT-6, pp. 52–57, Jan. 1988.

[27] B. M. A. Rahman and J. B. Davies, "Vector-H finite element solution of GaAs/GaAlAs rib waveguides," in Optoelectronics, IEE Proceedings J 132, 1985, pp. 349–353.

C. Pan received the B.Sc. Eng. Degree from the School of Electronic Science & Engineering, Southeast University, Nanjing, P. R. China in 2009. He is currently a Ph D student at Southeast University, Nanjing, P. R. China. In Nov. 2014, he was exchanged to City University, London, U.K., for 1 year mobility Ph D study sponsored by INTACT program.

B. M. A. Rahman (S'80–M'83–SM'94) received the B.Sc. Eng. and M.Sc. Eng. degrees (with distinctions) in electrical engineering from Bangladesh University of Engineering and Technology (BUET), Dhaka, Bangladesh, in 1976 and 1979, respectively, and the Ph.D. degree in electronics from University College London, London, U.K., in 1982.

From 1976 to 1979, he was a Lecturer in the Department of Electrical Engineering, BUET. In 1982, he was a Postdoctoral Research Fellow at University College London, where he continued his research on the development of finite-element method for characterizing optical guided-wave devices. In 1988, he joined City University, London, as a Lecturer, where he is now a Professor, and leads the research group on photonics modeling, specialized in the use of rigorous and full-vectorial numerical approaches to design, analyze, and optimize a wide range of photonic devices, such as spot-size converters, high-speed optical modulators, compact bend designs, power splitters, polarization splitters, polarization rotators, polarization controllers, terahertz devices, etc. He is the author or coauthor of more than 450 journal and conference papers, and his journal papers have been cited more than 3200 times.

Prof. Rahman received two gold medals for being the best undergraduate and graduate students of the university in 1976 and 1979, respectively. In 1979, he was awarded with a Commonwealth Scholarship to study for a Ph.D. degree in the U.K. He is a Fellow of Institute of Electrical and Electronic Engineers (IEEE), the Optical Society of America (OSA), and the Society of Photographic Instrumentation Engineers (SPIE).